Journal of Materials Chemistry B

PAPER

View Article Online
View Journal | View Issue

Cite this: J. Mater. Chem. B, 2014, 2, 4324

Microwave-assisted synthesis of hemin–graphene/poly(3,4-ethylenedioxythiophene) nanocomposite for a biomimetic hydrogen peroxide biosensor†

Wu Lei, Lihua Wu, Wenjing Huang, Qingli Hao,* Yuehua Zhang and Xifeng Xia

Received 25th February 2014
Accepted 7th April 2014

DOI: 10.1039/c4tb00313f

www.rsc.org/MaterialsB

The large-scale synthesis of ternary nanocomposite hemin–graphene sheets/poly(3,4-ethylenedioxythiophene) (H–GNs/PEDOT) was achieved *via* a microwave-assisted method, in which PEDOT was polymerized with graphene oxide and induced with hemin on the H–GNs nanosheets without additional oxidants; meanwhile, graphene oxide was partially reduced simultaneously. The morphology and structure of the as-prepared nanocomposites were characterized by transmission electron microscopy, Fourier-transform infrared spectroscopy, and ultraviolet-visible absorption spectroscopy. The H–GNs/PEDOT nanocomposite combines the main excellent properties of the three components, maintaining the peroxidase-like activity of hemin, and displaying a high-speed electron transfer ascribed to the presence of PEDOT and the graphene sheets. The H–GNs/PEDOT exhibited remarkable electrocatalysis towards the reduction of H_2O_2 due to the direct electron-transfer between the hemin and the modified electrode. The excellent synergic effect enables an enhanced electrochemical performance of the H–GNs/PEDOT modified electrode with good biocompatibility and fast redox property. The novel biomimetic H_2O_2 biosensor based on the well-designed ternary hybrid H–GNs/PEDOT has a low detection limit (0.08 μM) with a high dynamic response range (10^{-7} to 10^{-5} M) and a high sensitivity (235 μA mM^{-1} cm^{-2}). The sensor displays good selectivity, repeatability, reproducibility and stability.

1 Introduction

Hemin (iron protoporphyrin IX) is the active center of the heme-protein family, with members such as horseradish peroxide (HRP), myoglobin (Mb), hemoglobin (Hb), cytochrome c (Cyt c) and catalase (CAT), all being characterized in the well-known reversible redox reaction of Fe(III)/Fe(II). The most remarkable feature of hemin is its peroxidase-like activity similar to peroxidase enzyme and good electrocatalysis to some small molecules related to biological processes, including nitric oxide,[1] peroxynitrite,[2] oxygen,[3] and hydrogen peroxide.[4] As an artificial enzyme mimetic,[5] hemin has numerous advantages compared with traditional enzymes and precious metal catalysts, which are either extremely costly or easily influenced by environmental temperature, pH value and toxic chemicals.[6] However, to date, too many efforts have concentrated on exploring how to enhance the direct electrochemistry of heme proteins such as myoglobin[7,8] and hemoglobin[9–12] with deeply buried redox-active centers inside the proteins, ignoring the role of hemin itself, the actual active center of the heme-proteins. If we can obtain new hemin-based composites, an excellent level of direct electrochemistry may be conveniently achieved.

Recently, graphene or reduced graphene oxide (rGO)-based nanomaterials have raised considerable attentions in the fields of electrochemical sensors and biosensors, owing to the unique nanostructure of the graphene component and its resulting superior properties (large surface area, high thermal and electrical conductivity, ease of functionalization, *etc.*).[13] Even though previous studies have demonstrated that hemin can successfully be adsorbed at graphene oxide or graphene through non-covalent functionalization by π–π interaction of porphyrin ring and substrates,[14] attempts at combining hemin with graphene nanosheets (H–GNs) for electrochemical sensing analysis have not been adequately explored.[15–17]

Up to now, H–GNs hybrid has generally been utilized for the colorimetric detection of single-nucleotide,[15] and glucose.[17] However, direct electrochemical determination based on the H–GNs composite, a rapid economic and sensitive detection method used widely in clinical diagnosis and environmental analyses, has been rare.[16] The main reason for this is the non-conductivity of hemin.[18] So how to obtain graphene with the intrinsic peroxidase-like activity of hemin while simultaneously possessing an excellent electron transfer ability for electrochemical sensing analysis is quite challenging.

School of Chemical Engineering, Nanjing University of Science and Technology, Nanjing, 210094, China. E-mail: qinglihao@njust.edu.cn; haoqingli@yahoo.com; Fax: +86-25-84315190; Tel: +86-25-84315943

† Electronic supplementary information (ESI) available. See DOI: 10.1039/c4tb00313f

Poly(3,4-ethylenedioxythiophene) (PEDOT) is one of the most popular conducting polymers in biosensors due to its excellent conductivity, good chemical stability and biocompatibility.[19] And unlike most thiophene derivatives, PEDOT can be polymerized in both organic and aqueous solutions,[20] so the synthesis of PEDOT in aqueous solution enables its application in biosensors. Therefore, a bold idea that integrates H–GNs with PEDOT to form a novel sensing material comes to mind.

Herein, we introduce the PEDOT conducting polymer into H–GNs to fabricate a novel H–GNs/PEDOT nanocomposite through a simple microwave strategy. The conjugated hemin–graphene oxide acts as the initial precursor, in which graphene oxide is used as the oxidant of EDOT polymerization and hemin plays the role of catalyst. Accurate detection of hydrogen peroxide (H_2O_2) is of important practical significance because it is an essential intermediate in food and pharmaceutical industrial production, clinical and environmental analyses.[21] On the basis of this nanocomposite, a biosensor for the quantitative determination of H_2O_2 is developed. Significantly, the H–GNs/PEDOT nanocomposite combines the main excellent properties of the graphene, hemin and PEDOT components. H–GNs/PEDOT not only maintains the peroxidase-like activity of hemin that can catalyze the reduction of H_2O_2, but displays a high-speed electron transfer ascribed to the presence of PEDOT and graphene sheets. Furthermore, the sufficient accessible specific area of graphene also provides a superb opportunity for a high loading of hemin and PEDOT within the composite matrix. Finally, the possible synergistic effect of the good combination of these three components can facilitate the electrochemical sensing performance of the nanocomposite.

2 Experimental

2.1 Reagents

Hemin (ferriprotoporphyrin IX chloride, 98 wt%) and 3,4-ethylenedioxythiophene (EDOT) were purchased from Aladdin reagents and used as received without further purification. Graphene oxide was prepared from natural graphite (12 000 mesh) by a modified Hummers method described elsewhere.[22] The real H_2O_2 sample we used is commercially available contact lens cleaning solution (CIBA Vision, Canada) containing 3% H_2O_2. Disodium hydrogen phosphate (Na_2HPO_4), sodium dihydrogen phosphate (NaH_2PO_4) and hydrogen peroxide (30% w/w) were obtained from Nanjing Chemical Regents Co., Ltd. 0.1 mol L^{-1} phosphate buffer solution (PBS) was prepared from NaH_2PO_4 and Na_2HPO_4. Distilled water was used for all experiments. All other reagents were of analytical grade.

2.2 Synthesis of H–GNs/PEDOT composites

The microwave synthesis of H–GNs/PEDOT composites was carried out using a CEM Discover microwave machine using single mode. Firstly, the H–GNs hybrid was prepared as follows: 6.2 mg hemin was added into 4 mL homogeneous graphene oxide (GO) suspension (2.0 mg mL^{-1}), followed by the addition of 40 μL ammonia (pH 10.0) to get a dark reddish-brown solution. The mixture was stirred gently for overnight to allow conjugation between hemin and GO. Then, 50 mmol EDOT was added to the above resulting H–GNs suspension by vigorous stirring for 1.5 h. Then the resulting dispersion was transferred into a microwave vessel and fixed in the vessel holder. The maximum power setting was set as 300 W and the pressure limit was 250 psi. The microwave irradiation was set at 120 °C for 30 min. After the reaction was completed, the microwave reaction vessel was cooled to room temperature. The black H–GNs/PEDOT composite was obtained by filtering through a nylon membrane (0.22 μm), and could be redispersed in water by ultrasonication.

2.3 Electrode modification

Prior to use, a glass carbon electrode (GCE) (CH instruments, USA) of 3 mm diameter was sequentially polished using 1.0 μm, 0.3 μm, and 0.05 μm alumina/water slurry on a polishing cloth, followed by thorough rinsing with distilled water. After cleaning in ethanol and distilled water for 5 min by ultrasonication respectively, the obtained electrode was dried with a purified N_2 stream. Typically, 5 μL of 1.0 mg mL^{-1} H–GNs/PEDOT solution was added dropwise onto the GCE surface and then dried at room temperature to prepare the H–GNs/PEDOT/GCE.

2.4 Apparatus and measurements

Transmission electron microscopy (TEM) images were obtained using a JEM-2100 instrument (JEOL Co., Ltd., Japan). Fourier-transform infrared (FT-IR) spectra were recorded using a Nicolet IS-10 (Thermo Scientific Co., Ltd., USA). UV-vis absorption spectra were recorded using an Evolution 220 Series UV-vis Spectrophotometer (Thermo Scientific Co., Ltd., USA).

Electrochemical measurements were carried out with a CHI660D electrochemical workstation (Shanghai Chenhua Co., Ltd., China) coupled with a traditional three-electrode system, employing a platinum wire, a saturated calomel electrode (SCE), and the bare or modified electrodes as the counter, reference and working electrodes, respectively. Before the experiments, the buffer solution was bubbled with pure nitrogen for about 15 min to achieve a roughly anaerobic condition. All measurements were performed at room temperature (22 ± 0.5 °C).

3 Results and discussion

3.1 Characterization of H–GNs/PEDOT film

The morphology of the as-synthesized H–GNs/PEDOT composite was characterized by TEM. From Fig. 1A, we can see that the edge of the H–GNs/PEDOT film is a few layers of graphene nanosheets with a typical wrinkled sheet-like feature, and the nanosheet is almost transparent. What is situated in the center section is the cascading intertwined network structure of PEDOT, implying that PEDOT was successfully grown along the graphene surface. The inset of Fig. 1A shows that nanostructured PEDOT exhibits a spindle shape with an average length of 900 nm and a mid-width of around 120 nm. As shown in Fig. 1B, neither individual graphene sheets nor PEDOT agglomerates can be observed, indicating the uniform growth of PEDOT with similar scale on the graphene sheets. The results

also indirectly demonstrate that hemin as the trigger point or catalyst of PEDOT polymerization is uniformly adsorbed on the graphene sheets.[23] Energy dispersive X-ray spectroscopy confirmed that the content of hemin is about 30 wt% (data not shown here).

Evidence further demonstrating the successful synthesis of H–GNs/PEDOT was supplied by UV-vis spectroscopy. As shown in Fig. 1C, the spectrum of hemin ammonia solution contains a strong peak at 386 nm attributed to the Soret band, together with a group of weak peaks between 550 and 700 nm ascribed to the Q-bands. H–GNs display a similar spectrum to that of hemin solution in terms of the absorption band position and shape, which demonstrates the successful attachment and good bioactivity of hemin on graphene sheets.[15] It is noted that the difference in absorbance is ascribed to the different concentrations of hemin and H–GNs solution. A strong absorption at 254 nm for H–GNs/PEDOT nanocomposites is observed, which corresponds to the chemically reduced graphene oxide,[24] and the broad absorption at *ca.* 412 nm with a large bathochromic shift (27 nm) can also been seen, which arises from the Soret band of hemin. These findings prove the existence of the π–π interaction between graphene and the porphyrin ring, and are essentially identical to the previous report.[25] The interactions of a cationic porphyrin derivative with chemically converted graphene would result in a red shift of the porphyrin Soret band.

FT-IR spectroscopy can provide some useful information on the structure of the H–GNs/PEDOT composites. Fig. 1D shows the comparative IR spectra of PEDOT, H–GNs and H–GNs/PEDOT. The IR spectrum of synthesized PEDOT is roughly consistent with that reported in the literature.[20] A band at 1635 cm^{-1} and a band centered around 1352 cm^{-1} are attributed to the C=C and C–C stretching vibrations in the thiophene ring, respectively. Bands at 985, 841 and 683 cm^{-1} are assigned to the C–S bond vibration. The bands at 1228 and 1065 cm^{-1} are due to the stretching of the ethylenedioxy group. Additionally, the disappearance of a strong band at 890 cm^{-1} (the C–H bending mode of the EDOT monomer) in the FTIR spectrum of the H–GNs/PEDOT composite further demonstrates the formation of PEDOT chains with α,α′-coupling compared with PEDOT. The H–GNs/PEDOT composite displays a bathochromic shift from 1635 to 1569 cm^{-1}, which means that the conjugated PEDOT chain is probably doped with H–GNs as the dopant. It is notable that the position and shape of the vibrations for hemin in H–GNs/PEDOT are in reasonable agreement with those of the hemin standard spectrum and the H–GNs spectrum, suggesting that hemin retains its native integrated structure and electrocatalytic activity in the H–GNs/PEDOT composite. Moreover, compared with the Raman spectra of the single components, the broadened Raman peaks located in 1200–1600 cm^{-1} of the H–GNs/PEDOT also prove the combination of PEDOT with the graphene sheets and hemin (demonstrated in Fig. S1†). Above all, we can conclude that the expected H–GNs/PEDOT composite has been successfully synthesized.

3.2 Direct electrochemistry of hemin on the H–GNs/PEDOT/GCE

The direct electrochemical behavior of hemin on the H–GNs/PEDOT/GCE is investigated in 5.0 mM $[Fe(CN)_6]^{3-/4-}$ containing 0.1 M KCl by Electrochemical Impedance Spectroscopy (EIS) and Cyclic Voltammetry (CV) methods.

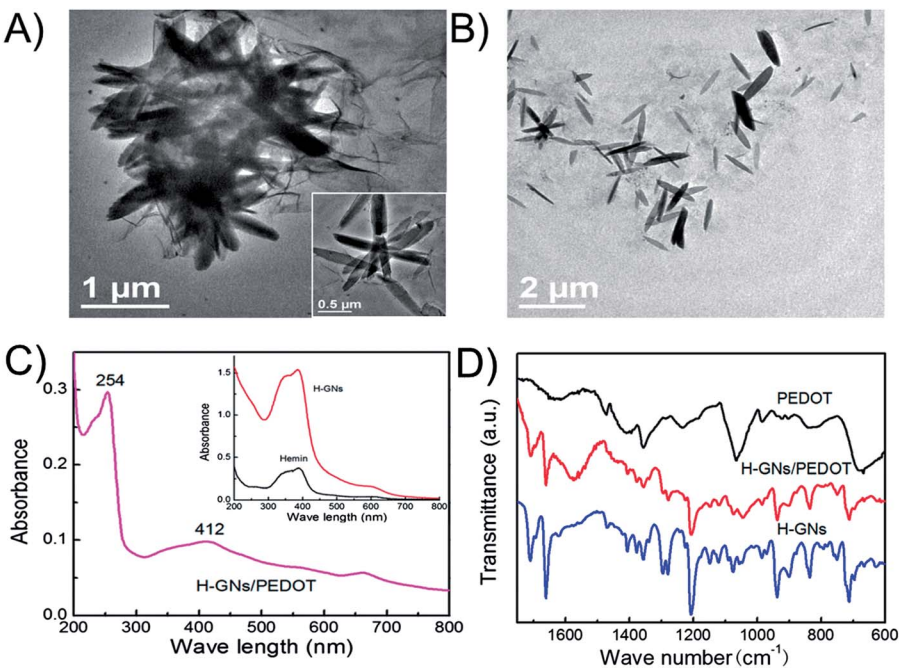

Fig. 1 TEM images (A and B) of the as-synthesized H–GNs/PEDOT composite. The inset is the high-magnification TEM of (A). UV-vis spectra (C) of hemin, H–GNs and H–GNs/PEDOT composite film. FTIR spectra (D) of PEDOT, H–GNs/PEDOT and H–GNs.

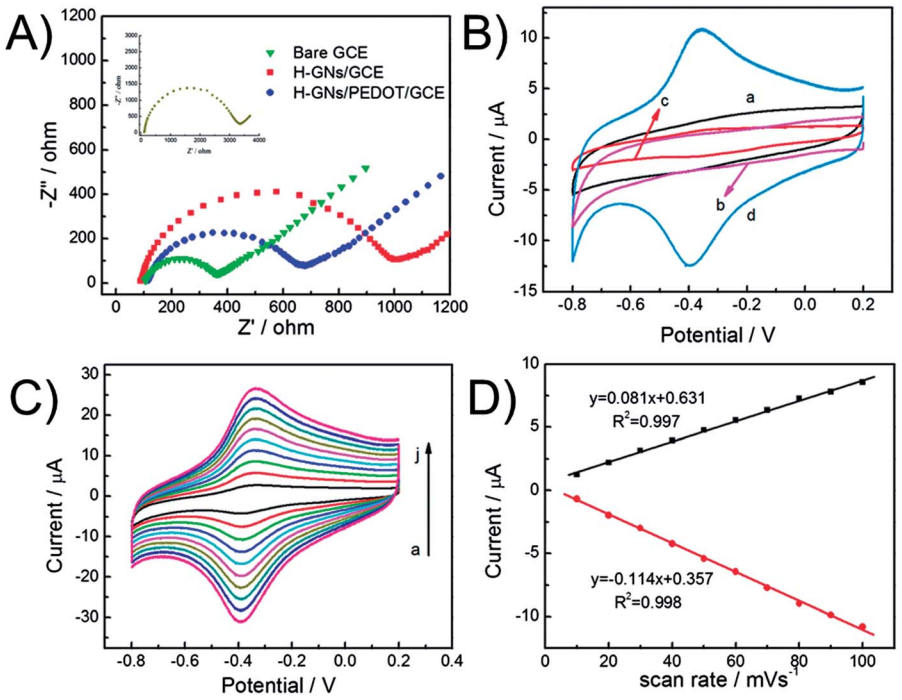

Fig. 2 (A) Nyquist plots of bare GCE, H–GNs/GCE, and H–GNs/PEDOT/GCE in 5.0 mM $[Fe(CN)_6]^{3-/4-}$ containing 0.1 M KCl. Frequency range: 0.1–10^6 Hz. Inset: Nyquist plot of hemin/GCE. (B) CVs of bare GCE (a), PEDOT/GCE (b), hemin/GCE (c), and H–GNs/PEDOT/GCE (d) in 0.1 M PBS. Scan rate: 100 mV s^{-1}. (C) CVs of H–GNs/PEDOT/GCE in 0.1 M PBS at different scan rates (a–j) from 10 to 100 mV s^{-1}. (D) Plots of anodic and cathodic peak currents *vs.* scan rate.

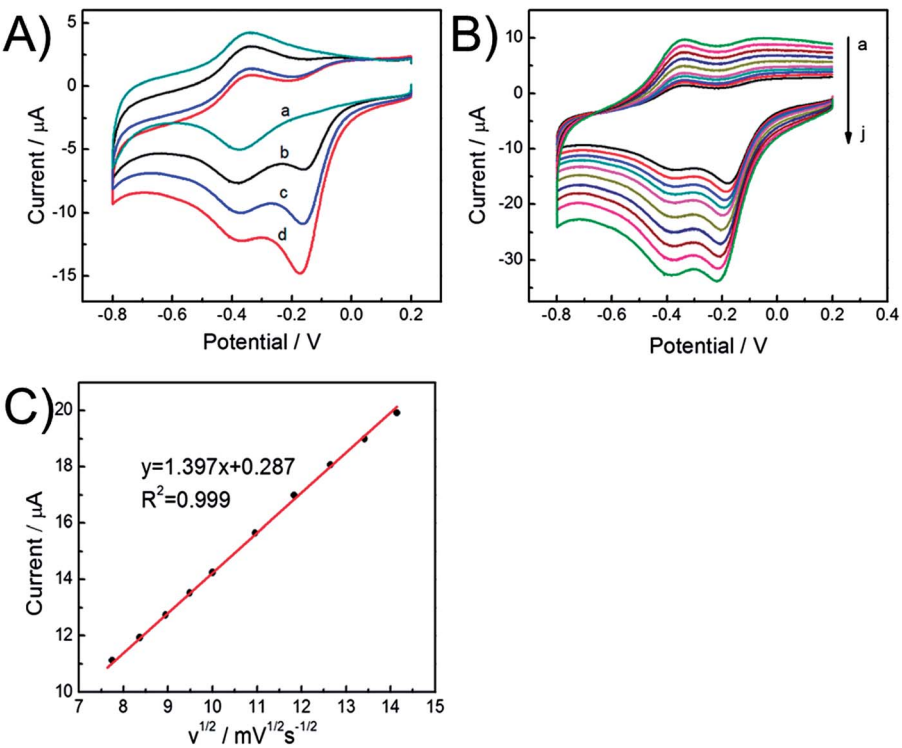

Fig. 3 (A) CVs of H–GNs/PEDOT/GCE in 0.1 M PBS (pH 7.0) containing (a) 0, (b) 0.5, (c) 1.0, and (d) 1.5 mM H_2O_2, respectively. Scan rate: 50 mV s^{-1}. (B) CVs of H–GNs/PEDOT/GCE in the presence of 1.5 mM H_2O_2 at varying scan rates from 60 to 200 mV s^{-1}. (C) The plot of cathodic peak currents *vs.* $v^{1/2}$.

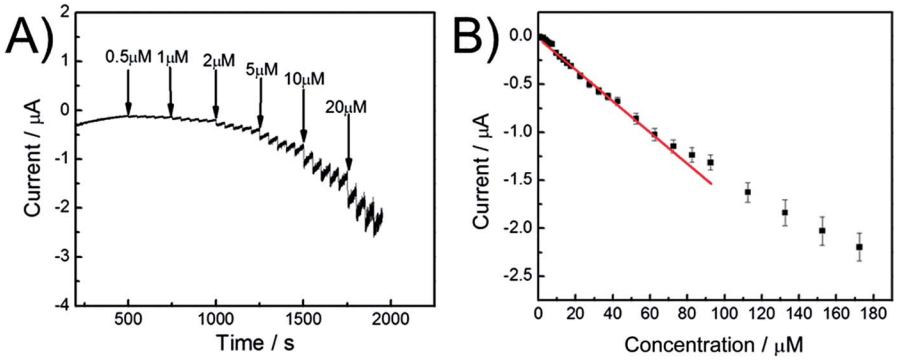

Fig. 4 (A) Amperometric response of H–GNs/PEDOT/GCE upon the successive addition of H_2O_2 at low concentrations (0.5, 1, 2, 5, 10, 20 μM) into gently stirred 0.1 M PBS. Applied potential: −0.2 V. (B) The plot of electrocatalytic current of H_2O_2 *vs.* the corresponding concentration. Error bars indicate standard deviations for three independent measurements at each H_2O_2 concentration.

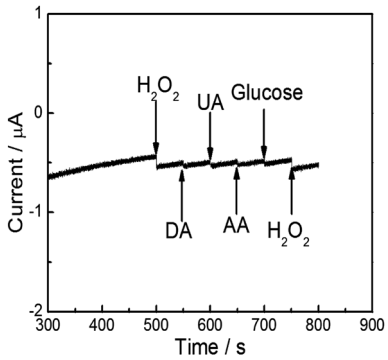

Fig. 5 Amperometric response of H–GNs/PEDOT/GCE at −0.2 V for the sequential addition of 1 μM H_2O_2, 10 μM DA, 10 μM UA and 10 μM AA, 10 μM glucose and 1 μM H_2O_2.

Table 1 The recovery determination of H_2O_2 in contact lens cleaning solution sample

	Real sample		
	Found (mM)		
Added (mM)	Mean[a]	RSD[b] (%)	Recovery (%)
4.9	4.96	8.8	101.2
9.8	9.51	7.7	97.0
19.6	19.71	3.7	100.6
29.4	29.73	3.2	101.1
53.9	53.79	3.1	99.8

[a] Average of three determinations. [b] Relative standard deviation.

As shown in Fig. 2A, the bare GCE shows a typical Nyquist plot which comprises a semicircle lying at high frequency related to the electron transfer-limited process in a film and a straight line nearly 45° at low frequency related to the diffusion-limited process. The inset of Fig. 2A shows a quite significant semicircle, which arises from the known non-conductivity of porphyrin. Compared with the plot of H–GNs/GCE, the H–GNs/PEDOT/GCE exhibits a lower electron-transfer resistance (R_{et}) determined by the diameter of the semicircle. It indicates that the PEDOT and graphene play important roles in accelerating the electron transfer between the electrolyte solution and electrode interface.

Fig. 2B shows the CVs of different modified electrodes in 0.1 M PBS. As expected, there were no redox peaks appearing for the bare GCE and PEDOT/GCE (curves a and b). When the bare GCE was modified with hemin, a couple of weak quasi-reversible redox peaks were seen (curve c), and the redox response is due to the single-electron-transfer process of iron at the inner of hemin.[15] Additionally, the background current of the hemin/GCE is smaller than that of the bare GCE, further demonstrating the successful immobilization of hemin. However, a pair of stable and well-defined redox peaks were observed at the H–GNs/PEDOT/GCE (curve d). Both the redox peaks and background current for the H–GNs/PEDOT/GCE were much bigger than those for the hemin/GCE and PEDOT/GCE. The anodic and cathodic peak potentials were located at −0.357 and −0.410 V, respectively, which resulted from direct electron transfer of the immobilized hemin for the conversion between Fe(III) and Fe(II). The peak-to-peak potential separation (ΔE_p) was 53 mV at a scan rate of 100 mV s^{-1}, much smaller than some other hemin modified electrodes reported,[26,27] implying a fast direct electron-transfer between the redox-active site of hemin and the modified electrode. Apparently, the presence and good synergy effect of graphene and PEDOT are decisive factors for the achievement of the rapid electron transfer of hemin.

Cyclic voltammograms of the H–GNs/PEDOT film-modified electrode at various scan rate are shown in Fig. 2C. The redox peak currents corresponding to hemin increased as a function of the scan rate. The cathodic and anodic peak currents increased linearly with the scan rate from 10 to 100 mV s^{-1}, indicating that hemin embedded in the H–GNs/PEDOT film underwent a surface-controlled process. For such a surface process, the surface concentration (Γ^*) can be estimated using the Laviron equation:[28]

$$I_p = \frac{n^2F^2\nu\Gamma^*A}{4RT}$$

where I_p is the peak current, n is the number of electron(s) transferred ($n = 1$), F is the Faraday constant, ν is the scan rate, A is the effective surface area (0.072 cm^2), R is the gas constant,

and T is the temperature (298.15 K). According to the slope of I_p *vs.* v, the surface concentration is calculated to be 1.22×10^{-9} mol cm^{-2}, which is larger than the theoretical monolayer coverage of hemin (6.89×10^{-11} mol cm^{-2}). It means that the surface area of the H–GNs/PEDOT film is efficiently enlarged through the combination of graphene and PEDOT chains to provide a cross-linked network structure for better loading of hemin and the analytes,[29] which can enhance the catalytic ability and faradaic response.

3.3 Electrocatalysis of H–GNs/PEDOT film towards H_2O_2

To investigate the electrocatalytic activity of the H–GNs/PEDOT/GCE towards H_2O_2, CV was employed over a potential range from −0.8 to 0.2 V. Fig. 3A shows the CVs of the H–GNs/PEDOT/GCE in 0.1 M PBS (pH7.0) in the presence of different concentrations of H_2O_2. Clearly, the CV of H–GNs/PEDOT/GCE only shows characteristic redox peak of hemin without H_2O_2. Upon addition of 0.5 mM H_2O_2, a new well-defined reduction peak centered at −0.162 V appears. Further increasing the concentration of H_2O_2 from 0.5 to 1.5 mM, the corresponding cathodic peak current increased progressively, indicating the occurrence of the typical electrocatalytic reduction process of H_2O_2. It is worth noting that the reduction potential of H_2O_2 is significantly lower than the values reported in the literature.[7,9,29] The low operation potential endows the H_2O_2 biosensor with a better sensitivity since it gives less exposure to interfering reactions, which is different from redox mediator-based sensors.[30] The reduction of H_2O_2 results from the electrocatalytic process of $hemin_{red}$, while $hemin_{red}$ itself is oxidized to $hemin_{ox}$ and then quickly reduced back to $hemin_{red}$ through its direct electron transfer with the electrode.[4]

Fig. 3B shows the CVs of the H–GNs/PEDOT/GCE recorded in 0.1 M PBS in the presence of 1.5 mM H_2O_2 at different scan rates. Obviously, the reduction peak current of H_2O_2 increases linearly with the square root of the scan rate in the range of 60–200 mV s^{-1} (Fig. 3C), indicating the diffusion-controlled process of H_2O_2.

As previously mentioned, the accurate and fast detection of H_2O_2 is of extreme importance. Herein, the determination of H_2O_2 on the H–GNs/PEDOT/GCE was investigated using an amperometric method. Fig. 4A shows a typical amperometric response of the H–GNs/PEDOT/GCE upon successive addition of a specific concentration of H_2O_2 into stirred 0.1 M phosphate buffer solution (pH 7.0) at regular intervals of 50 s. The applied potential (E_{app}) was held at −0.2 V *vs.* SCE. For every addition of H_2O_2, a well-defined and stable amperometric response was observed immediately, and achieved 95% steady-state current towards H_2O_2 within 3 s, indicating that the electrocatalytic reaction was sensitive and extraordinarily rapid. The response currents increased linearly with the concentration of H_2O_2 from 0.5 to 70 μM. The calibration curve for the H–GNs/PEDOT/GCE is shown in Fig. 4B. The linear regression equation is expressed as $I_p/\mu A = -0.0167 \times [H_2O_2]/\mu M + 0.00147$ ($R^2 = 0.985$). The sensitivity was calculated to be 235 μA mM^{-1} cm^{-2}.[31–33] The limit of detection (LOD) could reach as low as 0.08 μM based on the formula LOD = $3S_b/S$ (where S_b = standard deviation of blank signal and S = sensitivity).[7] The analytical performance of the proposed biosensor towards the determination of H_2O_2 is superior over some other reported heme-related sensors in terms of wide linear range, high sensitivity and low LOD.[16,32–34]

The selectivity of the obtained biosensor towards H_2O_2 was investigated with the interference of some common substances such as dopamine, uric acid, ascorbic acid and glucose. Fig. 5 represents the amperometric response for the successive addition of 1 μM H_2O_2 and 10-fold concentration of dopamine (DA), uric acid (UA), ascorbic acid (AA), glucose and 1 μM H_2O_2 at the H–GNs/PEDOT/GCE. A steady-state amperometric response was observed towards 1 μM H_2O_2, whereas no obvious responses, generally less than 2%, were obtained for the sequential addition of the above-mentioned interfering species. Again a well-defined amperometric response was also obtained with subsequent addition of 1 μM H_2O_2 into the above buffer solution. Thus the selective determination of H_2O_2 can be achieved even in the coexistence of high concentrations of common interfering species, revealing the excellent selectivity of the as-proposed biosensor based on the H–GNs/PEDOT/GCE.

The reproducibility, stability and repeatability of the sensor were also evaluated. Only a slight decrease of peak currents of about 7% could be seen from the CV curves after 100 cyclic scans in pH 7.0 PBS at 100 mV s^{-1}. When the electrode was stored at 4 °C and used again after three weeks, the current response corresponding to the hemin redox reaction showed only a 15% decrease of the original value, indicating good stability. The relative standard deviation (RSD) of the peak current in six successive determinations at a H_2O_2 concentration of 0.5 mM was 5.6% for the H–GNs/PEDOT/GCE. The good stability might be attributed to the good biocompatibility of the well-combined composite, to the synergistic effect and the unique properties of the three components. Five different modified GCEs were independently fabricated (using the same GC electrode), the peak current related to the redox reaction of hemin was tested by CV, and the corresponding RSD values determined were less than 5%. The repeatability of the modified electrodes was also acceptable.

To investigate the practical feasibility of the H–GNs/PEDOT/GCE biosensor, the commercially available contact lens cleaning solution containing 3% H_2O_2 was examined. The real sample was diluted with PBS (pH 7.0) to obtain the required H_2O_2 concentration shown in Table 1, and the amperometric experiment was performed with experimental conditions similar to the laboratory samples. The real sample results for contact lens cleaning solution (using standard addition method) are listed in Table 1.

4 Conclusions

The H–GNs/PEDOT nanocomposite was synthesized *via* a facile microwave-assisted method and its biomimetic sensing towards H_2O_2 was also investigated. We have described the fabrication a novel H_2O_2 biosensor consisting of a H–GNs/PEDOT composite film. The high performance of the H–GNs/PEDOT-modified GCE showed that PEDOT and graphene have an excellent synergic effect with hemin in stimulating the

electron transfer of hemin. Moreover, the hemin embedded in the composite film maintained good electrocatalytic activity towards hydrogen peroxide. The results of the electrochemical detection of H_2O_2 indicate that the H–GNs/PEDOT/GCE exhibits high sensitivity and a low detection limit towards the reduction of H_2O_2 compared with other related hemin-based sensors reported in the literature. Additionally, the low cost, very fast response time, good stability, repeatability and selectivity of the H–GNs/PEDOT-modified electrode make it a potential candidate for the fabrication of novel H_2O_2 biosensors. Moreover, in comparison to other nanomaterials, the environmentally-friendly, cost-efficient and large-scale production of H–GNs/PEDOT fabricated through the microwave approach also makes it a promising material for use in other biosensors.

Acknowledgements

The work was supported by the National Natural Science Foundation of China (no. 21103092), Program for NCET-12-0629, the Fundamental Research Funds for the Central Universities (no. 30920130111003), the Ph.D. Programs Foundation of Ministry of Education of China (no. 20133219110018), Qing Lan Project and Six Major Talent Summit (XNY-011), the Science and Technology Support Plan and PAPD of Jiangsu Province, China (nos BE2011835 and BE2013126).

Notes and references

1 R. M. Santos, M. S. Rodrigues, J. Laranjinha and R. M. Barbosa, *Biosens. Bioelectron.*, 2013, **44**, 152–159.
2 S. Peteu, P. Peiris, E. Gebremichael and M. Bayachou, *Biosens. Bioelectron.*, 2010, **25**, 1914–1921.
3 Z.-X. Liang, H.-Y. Song and S.-J. Liao, *J. Phys. Chem. C*, 2011, **115**, 2604–2610.
4 H. Song, Y. Ni and S. Kokot, *Anal. Chim. Acta*, 2013, **788**, 24–31.
5 L. Fruk and C. M. Niemeyer, *Angew. Chem., Int. Ed.*, 2005, **44**, 2603–2606.
6 A. Durkop and O. S. Wolfbeis, *J. Fluoresc.*, 2005, **15**, 755–761.
7 V. Mani, B. Dinesh, S. M. Chen and R. Saraswathi, *Biosens. Bioelectron.*, 2014, **53**, 420–427.
8 M. M. Barsan, E. M. Pinto and C. M. A. Brett, *Electrochim. Acta*, 2010, **55**, 6358–6366.
9 C. Guo, F. Hu, C. M. Li and P. K. Shen, *Biosens. Bioelectron.*, 2008, **24**, 825–830.
10 W. Sun, L. Cao, Y. Deng, S. Gong, F. Shi, G. Li and Z. Sun, *Anal. Chim. Acta*, 2013, **781**, 41–47.
11 X. He, L. Zhou, E. P. Nesterenko, P. N. Nesterenko, B. Paull, J. O. Omamogho, J. D. Glennon and J. H. Luong, *Anal. Chem.*, 2012, **84**, 2351–2357.
12 C. Zhao, L. Wan, L. Jiang, Q. Wang and K. Jiao, *Anal. Biochem.*, 2008, **383**, 25–30.
13 M. Zhou, Y. Zhai and S. Dong, *Anal. Chem.*, 2009, **81**, 5603–5613.
14 Y. Xu, Z. Liu, X. Zhang, Y. Wang, J. Tian, Y. Huang, Y. Ma, X. Zhang and Y. Chen, *Adv. Mater.*, 2009, **21**, 1275–1279.
15 Y. Guo, L. Deng, J. Li, S. Guo, E. Wang and S. Dong, *ACS Nano*, 2011, **5**, 1282–1290.
16 J. Chen, L. Zhao, H. Bai and G. Shi, *J. Electroanal. Chem.*, 2011, **657**, 34–38.
17 Y. Guo, J. Li and S. Dong, *Sens. Actuators, B*, 2011, **160**, 295–300.
18 Y. Zhou, M. Wang, X. Meng, H. Yin and S. Ai, *RSC Adv.*, 2012, **2**, 7140.
19 W. Si, W. Lei, Y. Zhang, M. Xia, F. Wang and Q. Hao, *Electrochim. Acta*, 2012, **85**, 295–301.
20 S. V. Selvaganesh, J. Mathiyarasu, K. L. N. Phani and V. Yegnaraman, *Nanoscale Res. Lett.*, 2007, **2**, 546–549.
21 L. C. Chang, H. N. Wu, C. Y. Lin, Y. H. Lai, C. W. Hu and K. C. Ho, *Nanoscale Res. Lett.*, 2012, **7**, 319.
22 H. Wang, Q. Hao, X. Yang, L. Lu and X. Wang, *Nanoscale*, 2010, **2**, 2164–2170.
23 Q. Sheng, M. Wang and J. Zheng, *Sens. Actuators, B*, 2011, **160**, 1070–1077.
24 J. Zhang, H. Yang, G. Shen, P. Cheng, J. Zhang and S. Guo, *Chem. Commun.*, 2010, **46**, 1112–1114.
25 Y. Xu, L. Zhao, H. Bai, W. Hong, C. Li and G. Shi, *J. Am. Chem. Soc.*, 2009, **131**, 13490–13497.
26 J. Wei, J. Qiu, L. Li, L. Ren, X. Zhang, J. Chaudhuri and S. Wang, *Nanotechnology*, 2012, **23**, 335707.
27 Q. Ma, S. Ai, H. Yin, Q. Chen and T. Tang, *Electrochim. Acta*, 2010, **55**, 6687–6694.
28 E. Laviron, *J. Electroanal. Chem. Interfacial Electrochem.*, 1979, **100**, 263–270.
29 G. Ran, W. J. Yi, Y. Li, H. Q. Luo and N. B. Li, *Anal. Methods*, 2012, **4**, 2929.
30 W. Chen, S. Cai, Q. Q. Ren, W. Wen and Y. D. Zhao, *Analyst*, 2012, **137**, 49–58.
31 S. Woo, Y.-R. Kim, T. D. Chung, Y. Piao and H. Kim, *Electrochim. Acta*, 2012, **59**, 509–514.
32 M.-Y. Hua, Y.-C. Lin, R.-Y. Tsai, H.-C. Chen and Y.-C. Liu, *Electrochim. Acta*, 2011, **56**, 9488–9495.
33 K.-P. Lee, A. I. Gopalan and S. Komathi, *Sens. Actuators, B*, 2009, **141**, 518–525.
34 X. Che, R. Yuan, Y. Chai, L. Ma, W. Li and J. Li, *Microchim. Acta*, 2009, **167**, 159–165.

